# Canopy Architecture and Remote Sensing of the Fraction of Photosynthetically Active Radiation Absorbed by Boreal Conifer Forests

Jing M. Chen

*Abstract*—**Measurements of the fraction of photosynthetically active radiation (FPAR) absorbed by the forest overstory were made at 20 sites in black spruce (*Picea mariana*) and jack pine (*Pinus banksiana*) boreal forests located in Saskatchewan and Manitoba, Canada. Canopies of both species have similar vertical tree crown structure but different branch and shoot architecture. Intensive investigation was made on the effect of these canopy architecture on the penetration of total visible radiation into the canopy at various solar zenith angles $\theta$, quantified using the projection coefficient $G_t(\theta)$. Based on experimental evidence, constant values of $G_t(\theta)$ and the above- and below-canopy PAR reflectivities are suggested for these two species for the calculation of daily green FPAR. The calculation then requires only a single stand parameter: the effective green leaf area index (LAI) $L_{eg}$, which is similar to the effective LAI $L_e$ measured using optical instruments but reduced by a small fraction to remove the contribution of woody material to the total above-ground plant area. Daily green FPAR of the sites was correlated with the Simple Ratio (SR) and the Normalized Difference Vegetation Index (NDVI) obtained from Landsat 5 TM images. The correlation was better in late-spring than in mid-summer, suggesting spring images are more useful for obtaining FPAR of the overstory. Comparisons of the present with previous results suggest that the background (understory and ground cover) signal and the tree crown shadows are important in satellite measurements of FPAR.**

## I. Introduction

BOREAL ecosystems may be one of the keys to the unresolved global carbon budget problem [1]. Numerical models for the carbon cycle and biogeochemistry in boreal ecosystems and their interaction with atmosphere [2]–[5] require remote sensing data to provide quantitative coverage for large areas. The key remote sensing input to models of this kind includes leaf area index (LAI) and the fraction of photosynthetically active radiation (FPAR) absorbed by vegetated surfaces. In the models, FPAR allows the calculation of the PAR absorbed (APAR) by a plant canopy from satellite-derived incident PAR (IPAR) and is critical in estimating photosynthesis, respiration, and other biological processes in the canopy. In the case of forest stands, it can also be used to estimate the radiative energy reaching the forest floor and affecting soil microbic activities contributing to the carbon cycle. This paper reports results from a study as part of Boreal Ecosystem-Atmosphere Study (BOREAS), which aims at understanding the functionalities of boreal ecosystems and their role in global carbon budget [6].

Vegetation indexes used for deriving FPAR from remote sensing data are formulated based on reflectance of solar radiation in red and near infrared wavebands, denoted by $\rho_r$ and $\rho_n$, respectively. A number of two-band vegetation indexes have been proposed for vegetation studies. Among them, the Normalized Difference Vegetation Index (NDVI) [7], $(\rho_n - \rho_r)/(\rho_n + \rho_r)$, and the simple ratio (SR) [8], $\rho_n/\rho_r$, have been most frequently used in the past and still remain the major intermediate variables to obtain the global coverage of biophysical parameters [9]–[11]. Chen [12] found that NDVI and SR are better correlated to overstory LAI and FPAR in boreal forests than many other vegetation indexes including the Soil Adjusted Vegetation Index (SAVI) [13], Modified SAVI (MSAVI) [14], Weighted Difference Vegetation Index (WDVI) [15], Global Environment Monitoring Index (GEMI) [16], Non-Linear Index (NLI) [17], and Renormalized Difference Vegetation Index (RDVI) [18]. NDVI and SR are therefore selected in this study.

The functional relationship between FPAR and NDVI or SR have been investigated using canopy radiative transfer models [19]–[21]. Experimental data for the relationship are reported for wheat [22], grass [23], alfalfa [24], and temperate forests and grassland [25]. Global digital maps of FPAR have been produced based on simple linear relationships between FPAR and SR (calculated from NDVI) for various vegetation types because of lack of data for many natural ecosystems [9]. Among them, boreal forests are of great importance in terms of their spatial coverage and their role in global carbon budget and climate change.

The problem with the scarcity of boreal field data is exacerbated by the difficulty in modeling the radiative transfer processes in boreal ecosystems. Boreal forests have their distinct canopy architecture: relatively even age, open, and highly organized. They also have abundant understory and moss ground cover which are considerably different from low-NDVI soil background in agroecosystems. Conifer canopies, in particular, have several foliage architectural levels: shoots, branches, whirls, tree crowns and tree groups [26]. All these architectural hierarchies affect the radiative transfer processes within the canopies and contribute to remotely observed reflected solar radiances. With about 0.5–1.5 million needles on a single tree, which may be distributed in different patterns, it would be almost impossible to model the radiative regimes

Manuscript received August 10, 1995; revised January 26, 1996.

The author is with the Applications Division, Canada Centre for Remote Sensing, Ottawa, Ontario, Canada K1A 0Y7 (e-mail: chen@ccrs.nrcan.gc.ca).

Publisher Item Identifier S 0196-2892(96)06812-X.

by radiosity such as DIANA [27] or using complete three-dimensional (3-D) foliage description [28]. The simpler model of Li and Strahler [29] or others alike, which consider the tree crown shape in describing the radiative transfer processes, would be practically more useful for conifer stands. Numerical models, however sophisticated, are only simplified mathematical descriptions of the complicated physical reality and need validation and improvements based on field data.

In order to obtain ground-truth LAI and FPAR data for spatially heterogeneous boreal forests, we developed an optical instrument named Tracing Radiation and Architecture of Canopies (TRAC) [30] [31]. This instrument enables us to acquire the average transmitted PAR through the canopy and the reflected PAR from the forest floor over long transects which are critical to FPAR estimation. The objectives of this paper are: 1) to provide an effective way for estimating FPAR for conifer canopies with distinct foliage architecture, 2) to investigate the various components affecting FPAR, and 3) to fill in the data gap for boreal forests in the NDVI-FPAR relationship.

## II. Theory

### A. Instantaneous FPAR

FPAR is defined as the fraction of IPAR which is absorbed by the canopy [19]. In this study, the canopy is defined as the overstory of the forest stand. By this definition, FPAR excludes the fraction of PAR reflected by the canopy and the fraction absorbed by the underlying surface including the soil, ground cover, and understory but includes the small fraction of PAR which is absorbed by the canopy after the reflection by the underlying surface. To obtain FPAR, it is therefore required to measure the downwelling and upwelling PAR at two levels: immediately above and below the canopy. When such measurements at time $t$ are available, the instantaneous FPAR, denoted by $F(t)$, is then calculated as follows:

$$F(t) = \frac{(P_{d1} - P_{u1}) - (P_{d2} - P_{u2})}{P_{d1}} \tag{1}$$

where $P_{d1}$ and $P_{u1}$ are the downwelling (incident) and upwelling (reflected) PAR at level one (above the canopy), respectively; $P_{d2}$ and $P_{u2}$ are the corresponding terms at level two (below the canopy). In this equation, the fraction of PAR that is absorbed by the canopy after reflection by the underlying surface is also considered. After taking the ratio of the downwelling and upwelling irradiance at the same level, (1) can be rewritten as

$$F(t) = (1 - \rho_1(t)) - (1 - \rho_2(t))\frac{P_{d2}}{P_{d1}} \tag{2}$$

where $\rho_1(t)$ and $\rho_2(t)$ are, respectively, the PAR reflectivity above and below the canopy. Since the reflectivities are small and generally do not vary much between different types of stands, (2) demonstrates that the major task in measuring FPAR is to obtain $P_{d2}$ and $P_{d1}$ simultaneously. While the above stand $P_{d1}$ does not vary spatially under clear conditions and can be measured with a stationary sensor or predicted when data are missing, the below canopy $P_{d2}$ is highly variable in space and time and much more effort is needed to obtain the spatially averaged values. However, the ratio of $P_{d2}$ to $P_{d1}$ is closely related to canopy gap fraction and can be estimated from LAI, denoted by $L$, and other information on the foliage angle and spatial distribution patterns. Canopy gap fraction, $P(\theta)$ at the zenith angle $\theta$, can be calculated using the following equation [32]:

$$P(\theta) = \exp[-G(\theta)\Omega L/\cos\theta] \tag{3}$$

where $G(\theta)$ is the projection coefficient, being a constant of 0.5 for a spherical (random) distribution of foliage inclination angle. $L$ is defined as half the total leaf area per unit ground surface area [33]. $\Omega$ is a parameter determined by the spatial distribution pattern of foliage. Leaves in forest canopies are usually grouped at various scales, resulting in larger gap fractions than the random case, and hence $\Omega$ is smaller than unity and called the foliage clumping index. Generally $G(\theta)$ is unknown, and multiple angle measurements on gap fraction $P(\theta)$ are required to obtain $G(\theta)$ and $\Omega L$ simultaneously [34], [35]. Since $\Omega L$ is easily obtained from $P(\theta)$ measurements and is the essential canopy attribute determining the light environment, it has been called the effective LAI, denoted by $L_e$ [35]. In other words, it is $L_e$ rather than LAI that determines the gap fraction and FPAR.

The canopy gap fraction $P(\theta)$ equals the probability of solar beam penetration through the canopy, and hence (3) is readily used for estimating the direct radiation beneath the canopy. However, $P_{d1}$ and $P_{d2}$ required for the FPAR calculation are the total downwelling PAR including the direct and diffuse components. The transmission coefficients for diffuse and direct radiation are considerably different. The diffuse radiation transmission coefficient is not only determined by $G(\theta)$ and $L_e$ but also by leaf optical properties [36]. Plant leaves reflect and transmit direct and diffuse visible radiation, and therefore convert a fraction of IPAR into diffuse PAR through multiple scattering, compensating the decrease in the transmitted diffuse PAR from the sky. This effectively makes the extinction coefficient for diffuse radiation smaller than that for direct radiation [37]. The multiple scattering processes are determined not only by the leaf optical properties but also by canopy architecture and have been modeled with varying degrees of success [38] [28]. In this study, the multiple scattering effect is considered in the simplistic way

$$\frac{P_{d2}}{P_{d1}} = \exp[-G(\theta)\beta L_e/\cos\theta] \tag{4}$$

where $\beta$ is a parameter incorporating the scattering effect into the calculation and is determined by the foliage optical properties and structure. Because of the enhancement of diffuse radiation by multiple scattering, $P_{d2}/P_{d1}$ is always larger than the canopy gap fraction, leading to $\beta < 1$. The value of $\beta$ also depends on solar zenith angle because the percentage of diffuse PAR in the total PAR increases as the zenith angle increases. By combining (2) and (4), and expressing FPAR more generally as a function of $\theta$, we have

$$F(\theta) = (1 - \rho_1(\theta)) - (1 - \rho_2(\theta))\exp[-G_t(\theta)L_e/\cos\theta] \tag{5}$$

where

$$G_t(\theta) = \beta G(\theta) \tag{6}$$

$G_t(\theta)$ may be considered as the projection coefficient for total PAR transmission. The strategy of this study is to determine $G_t(\theta)$ for several intensive sites and apply species-specific $G_t(\theta)$ to other auxiliary sites.

$L_e$ can be measured using optical instruments. In forest stands, the measurements are usually made near the ground surface. $L_e$ measured this way is therefore affected by the area of all materials about the sensor including live and dead leaves, branches, boles, and their attachments such as moss and lichen. In order to calculate FPAR due to the green leaves only, i.e. green FPAR denoted by $F_g(\theta)$, the contribution of nongreen materials to $L_e$ should be removed. We replace $L_e$ in (5) with the effective green LAI, denoted by $L_{eg}$, to calculate $F_g(\theta)$ as follows:

$$F_g(\theta) = (1 - \rho_1(\theta)) - (1 - \rho_2(\theta)) \exp[-G_t(\theta) L_{eg} / \cos\theta] \tag{7}$$

$L_{eg}$ is defined as

$$L_{eg} = (1 - \alpha) L_e \tag{8}$$

where $\alpha$ is the ratio between nongreen (woody) area to the total area including green and nongreen areas. Values of $\alpha$ obtained by Chen [26] through destructive sampling for the same stands were used in this study. An implicit assumption made in using $L_{eg}$ this way is that the woody material with the area $\alpha L_e$ is located below the green leaves with the area $(1 - \alpha)L_e$. In reality, live branches and part of the tree trunk are located above some green leaves and have almost equal share of light with them. However, our destructive measurements in several conifer stands show that over two thirds of the woody surface area (tree trunks and dead branches) are located below the live tree crown, and therefore the error caused from making such an assumption is estimated to be less than 3% in FPAR if the proportion of the woody area to the total area is accurately determined.

Fig. 1 shows the diurnal variation of FPAR calculated using (5) for various $L_{eg}$ values with constant $\rho_1(\theta)$, $\rho_2(\theta)$, and $G_t(\theta)$. These constants are found from experiments to be most suitable for boreal black spruce stands. Because the pathlength of the solar beam increases with $\theta$, the diurnal variation in FPAR is pronounced, especially for canopies with low $L_{eg}$ values. This suggests that some attention must be given to obtaining daily FPAR from instantaneous FPAR. The shape of FPAR at $\theta > 75°$ is uncertain because data for $\rho_1(\theta)$ in these range is not available. However, because the instantaneous FPAR at large $\theta$ values has little contribution to the daily FPAR, constant $\rho_1(\theta)$ is assumed for the whole angle range.

The calculations are done for the whole canopy. For vertical distribution of FPAR within the canopy, $L_{eg}$ needs to be expressed as a function of height. In detailed photosynthesis estimation, FPAR variation with increment of LAI into the canopy is of interest, and (7) can be used for this purpose if the height dependence of $\Omega$ and $G_t(\theta)$ is ignored.

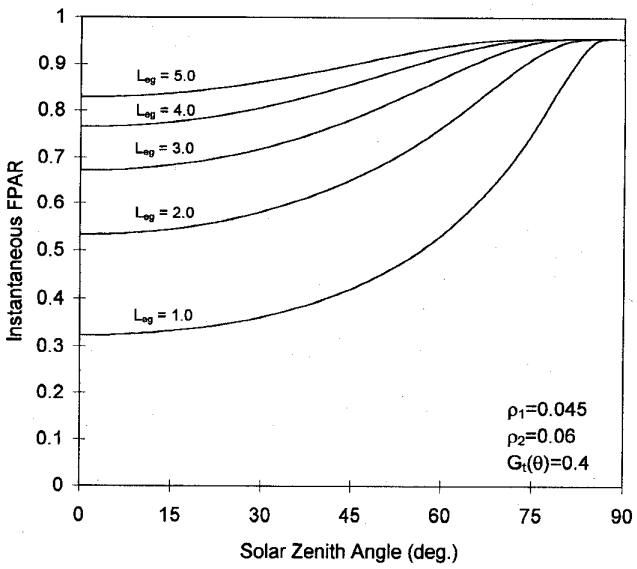


Fig. 1. Diurnal variation of instantaneous FPAR calculated using (7) at several fixed values of the effective green LAI ($L_{eg}$) with the constant input of PAR reflectivity at the top of the canopy ($\rho_1$) and at the bottom of the canopy ($\rho_2$), and the projection coefficient ($G_t(\theta)$) for the total (direct and diffuse) PAR.

### B. Daily Green FPAR

Because the instantaneous FPAR varies with the time of the day, it would be desirable to relate vegetation indexes to the stable daily values. In order to obtain daily green FPAR, denoted by $F_{gd}$, which can be used to convert daily IPAR into daily APAR, it is necessary to apply a weighting scheme to $F_g(\theta)$ as follows:

$$F_{gd} = \frac{\int_{\theta_{\min}}^{\pi/2} F_g(\theta) P_{d1}\, d\theta}{\int_{\theta_{\min}}^{\pi/2} P_{d1}\, d\theta} \tag{9}$$

where $\theta_{\min}$ is the solar zenith angle at noon. In (9), the integrations are presented with respect to $\theta$ rather than the time $t$ because they are approximately linearly related by $\cos\theta = \sin\phi \sin\delta + \cos\phi \cos\delta \cos[(t - 12)\pi/12]$ [39], where $\phi$ is the latitude; $\delta$ is the solar declination (little change in a day); and $t$ is the solar time in decimal hours. The integration is done with respect to solar zenith angle rather than solar solid angle under the assumption of the azimuthal uniformity of the canopy architecture. To simplify the calculation, we assume $P_{d1}$ is proportional to $\cos\theta$, i.e., $P_{d1} = P_0 \cos\theta$, where $P_0$ is the maximum PPFD at solar noon. With this assumption, (9) becomes

$$F_{gd} = \frac{\int_{\theta_{\min}}^{\pi/2} F_g(\theta) \cos\theta\, d\theta}{\int_{\theta_{\min}}^{\pi/2} \cos\theta\, d\theta} = \frac{1}{1 - \sin\theta_{\min}} \int_{\theta_{\min}}^{\pi/2} F_g(\theta) \cos\theta\, d\theta. \tag{10}$$

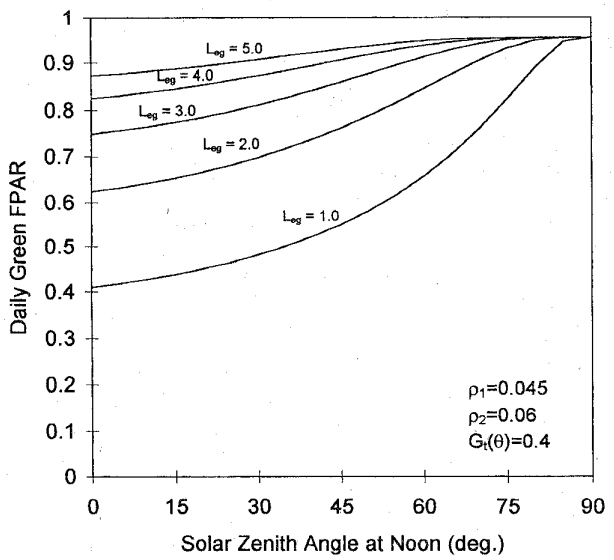


Fig. 2. The dependence of daily green FPAR calculated from (10) on the minimum solar zenith angle at noon at several effective green LAI ($L_{eg}$) values.

In this $\cos\theta$ weighting scheme, larger weights are given to smaller $F_g(\theta)$ values when the solar irradiance is higher during the day. Equation (10) simplifies the complete calculation involving integrations with respect to time and a weighting scheme with respect to the IPAR above the stand ($P_{d1}$).

Equation (10) shows that daily FPAR in a canopy with the same $L_{eg}$ depends on the height of solar trajectory at a given date and location. For conifer stands, $L_e$ is less variable than LAI, with the annual variations being less than 5% [26]. This is because the foliage clumping within the shoots varies with new growth in the spring and senescence in the fall [26]. The small seasonal variation in $L_e$ implies that FPAR for conifer stands at high latitudes can be larger in winter than in summer. Fig. 2 shows the dependence of daily green FPAR on solar zenith angle at noon for several $L_{eg}$ values. As expected from Fig. 1, the dependence is strong at small $L_{eg}$ values and becomes weaker as $L_{eg}$ increases, suggesting that considerable biases would result from assuming constant FPAR for open boreal forests.

## III. Field Data Collection

Field measurements of FPAR were made in black spruce (*Picea mariana*) and jack pine (*Pinus banksiana*) stands located in BOREAS Southern Study Area (SSA) near Candle Lake, Saskatchewan, and Northern Study Area (NSA) near Thompson, Manitoba, at the beginning, middle and end of the growing season in 1994 corresponding to the BOREAS Intensive Field Campaigns (IFC-1, IFC-2 and IFC-3, Sellers *et al.* 1995). IFC-1 (24 May–16 June) and IFC-2 ( 19 July–8 August) are referred to as late spring and mid-summer respectively. This paper uses measurements made in six intensive sites and 14 auxiliary sites. The intensive sites are BOREAS tower flux sites with a micrometeorological flux tower. They are SOJP (south old jack pine), SYJP (south young jack pine) and SOBS (south old black spruce) in the SSA, and likewise NOJP, NYJP, and NOBS in the NSA. At each intensive site, three parallel transects of equal length ranging from 150 m to 340 m were used for optical measurements. They were separated by 10 m and oriented in the southeast and northwest direction. At each auxiliary site, two perpendicular 50 m transects were established. The transects were oriented in north-south and east-west directions and crossed in the middle to form a + shape. Along each transect at both the intensive and auxiliary sites, a forestry flag was placed every 10 m to serve as a distance marker. The transmitted PAR through the canopy and the reflected PAR from the forest floor (moss, soil and understory) were measured using the TRAC along the transects on clear days. The instrument consists of three quantum sensors (LI-COR, Lincoln, NE, Model LI-190SB, 10 ms time constant), a data logger (Campbell Scientific, Logan, UT, Model CR10) and a storage module (Model SM716). Two of the sensors measure the downwelling total and diffuse PAR, and one measures the upwelling PAR either near the forest floor or above the forest top. The sensors were supported by a holding arm and sampled at a frequency of 32 Hz. The whole system was hand-carried by a person walking along the transects. With a walking pace of 1 m every three seconds, a sampling interval of 10 mm for each sensor could be achieved. These closely spaced measurements are used for both obtaining good spatial averages of PAR and studying the canopy architecture. The effective LAI was measured along the transects every 10 m using LI-COR LAI-2000. The instrument measures the transmittance of diffuse blue light from the sky simultaneously at five zenith angles, from which to calculate the effective LAI. To estimate the effect of blue light scattering on the $L_e$ measurements, TRAC measurements made at multiple angles were also used to calculate $L_e$. TRAC was also used periodically at the top of the flux tower to measure the downwelling and upwelling PPFD. Half hourly mean values of these quantities were also obtained from stationary LI-COR quantum sensors mounted on the tower by the tower flux research groups and were used for comparison with TRAC measurements. To investigate the effect of canopy architecture on PAR transmission through the canopies, the zenith angle of the main axis of shoots was measured using a simple device consisting of a protractor and a string. During measurement, the protractor was placed on the plane parallel with the shoot main axis and held vertically with a thin and rigid bar. The string was then run in the direction of the shoot main axis from the centre, indicating the zenith angle on the protractor. The measurements were made *in situ* for the short trees in SYJP and NYJP and on sections of tree crowns held vertical on the ground in SOBS.

The geographic locations of the stands required in satellite image processing were determined using a dual-receiver global positioning system (Trimble Pathfinder) with a nominal absolute accuracy of 10 m. However, the accuracy deteriorated substantially when the measurements were taken in closed stands with a portable antenna extended to just below tree crowns. The error for closed stands is estimated to be about $\pm 100$ m. This large error occurred for about three sites. For these sites, road maps with site locations provided by the

BOREAS staff team were used to assist in locating them in the image according to road turning features and distance from the road.

## IV. Satellite Image Processing

Vegetation indexes for the sites were obtained from four Landsat TM scenes at a spatial resolution of 30 m. Two scenes cover part of the BOREAS southern study area near Candle Lake, Saskatchewan (row number: 37/22–23, and dates: 6 June 1991 and 11 August 1986 with solar zenith angles of 35.9° and 43.2°, respectively), and the other two cover the northern study area located in between Nelson House and Thompson, Manitoba (row number 34/21, and dates: 9 June 1994 and 19 August 1985 with solar zenith angles of 37.3° and 43.9°, respectively). The June images were the most recent clear sky data, and the August images were acquired eight and nine years ahead of the field data collection because of limited data availability for this investigation. All the sites investigated are mature forests more than 50 years old except for the two 29-year-old young jack pine stands (SYJP and NYJP) [40]. We expect the change in the vegetation conditions within the nine year period to be small for all the sites.

The images were provided in a systematically georeferenced format [41]. Pixel registration of the images was accurate to within one pixel using over 20 ground control points. Radiometric corrections were made using coefficients (gains and offsets) provided with the images to convert the digital numbers into radiances. Simple cross-image atmospheric corrections were made using the "5s" model [42][43]. The model also provides output for calculating reflectances at the top and bottom of the atmosphere. NDVI and SR used in this study is calculated using the reflectance in TM band three (red) and four (near infrared) at the surface level after atmospheric corrections. In running the model, the options of continental airmass, midlatitude summer, and uniform targets were chosen, and the atmospheric visibility was set to 30 km for these cloudless scenes. It was found that the model output was not sensitive to the visibility larger than 10 km and the type of targets chosen. The average NDVI value for a site was taken from nine pixels in a square for the auxiliary sites and from 7–9 pixels on a line oriented in the northwest and southeast direction for the intensive sites to match the ground transects.

## V. Results and Discussion

### A. Ground Measurements

Fig. 3(a)–(c) are examples of TRAC measurements in SOBS, NOBS, and SOJP stands. Only 20 m data are shown to illustrate the spatial variability of downwelling total PPFD and reflected PPFD from the forest floor. The variation in PPFD transmitted through the canopy is characterized by a number of large flat-top spikes in between tree crowns and numerous small sharp spikes within tree crowns [26]. PPFD reflected from forest floor also exhibits considerable variation, showing gentle ridges and troughs corresponding to the increase or decrease in the transmitted PPFD. With such variability, it is difficult, or nearly impossible, to obtain good spatial averages with stationary sensors. Mobile sensors are an effective way to measure the average transmitted PAR over large areas in short durations.

Fig. 4(a)–(c) show examples of PAR measurements on clear days above and beneath SOBS, NOBS and SOJP canopies. The above-stand measurements are half hourly means of downwelling PAR obtained from stationary LI-COR quantum sensors mounted on the flux tower. The below-canopy measurements were made using the TRAC, each point being the mean of about 30 000 data points along a 300 m transect in SOBS and NOBS or 20 000 data points along a 200 m transect in SOJP. During the intensive field campaigns in the summer of 1994, there were only several similar clear days in both SSA and NSA. The TRAC measurements were used for calculations of not only FPAR but also foliage clumping index for improving the estimation of LAI [26]. The transect measurements were made only when the solar azimuth angle was at an angle greater than 30° to the transect to avoid sampling along long sunflecks or long shadows of tree crowns. This prevented us from obtaining the complete diurnal data beneath the canopy on the same transect. However, half-day data are sufficient to assess the effect of solar zenith angle with these long transects since the diurnal variation should be symmetrical about solar noon. It is noted that the total downwelling PPFD rapidly decreased in the afternoon due to the increase in the pathlength of the solar beam through the canopy, while the diffuse PPFD beneath the canopy showed much smaller changes with time, indicating the difference in the direct and diffuse radiation transfer processes in the canopies. It is also worth noting that the diffuse PPFD is larger in SOJP than in SOBS and NOBS (similar difference were found in other jack pine and black spruce stands), suggesting higher scattering coefficients for jack pine needles.

The above and below canopy PPFD measurements were used to calculate the "projection coefficient" $G_t(\theta)$ for the total downwelling PPFD (Fig. 5) using the following equation:

$$G_t(\theta) = \frac{\cos\theta}{L_e} \ln \frac{P_{d1}}{P_{d2}} \tag{11}$$

where $P_{d1}$ and $P_{d2}$ are above and below stand downwelling PPFD, respectively. $L_e$ is calculated from [44]

$$L_e = 2\int_0^{\pi/2} \ln(P_{D1}/P_{D2}) \cos\theta \sin\theta \, d\theta \tag{12}$$

where $P_{D1}$ and $P_{D2}$ are the downwelling direct PPFD above and below the canopy, respectively. $P_{D1}$ is taken as the difference between $P_{\max}$ and the diffuse PPFD beneath the canopy, where $P_{\max}$ is the maximum PPFD measured beneath the canopy, i.e., the total PPFD measured in the largest gap along the transect where the sensor is fully exposed to the sun. $P_{D2}$ is the mean of the difference between the instantaneous total downwelling PPFD and the diffuse PPFD beneath the canopy. As indicated in (12), the calculation of $L_e$ requires data of $P_{D1}/P_{D2}$ over the full solar zenith angle range from 0 to $\pi/2$. In reality, this is impossible because the minimum solar zenith angle is determined by the latitude and the solar declination. A linear curve fitting technique [45] was used to extend the measurements to the full angle range. For jack pine

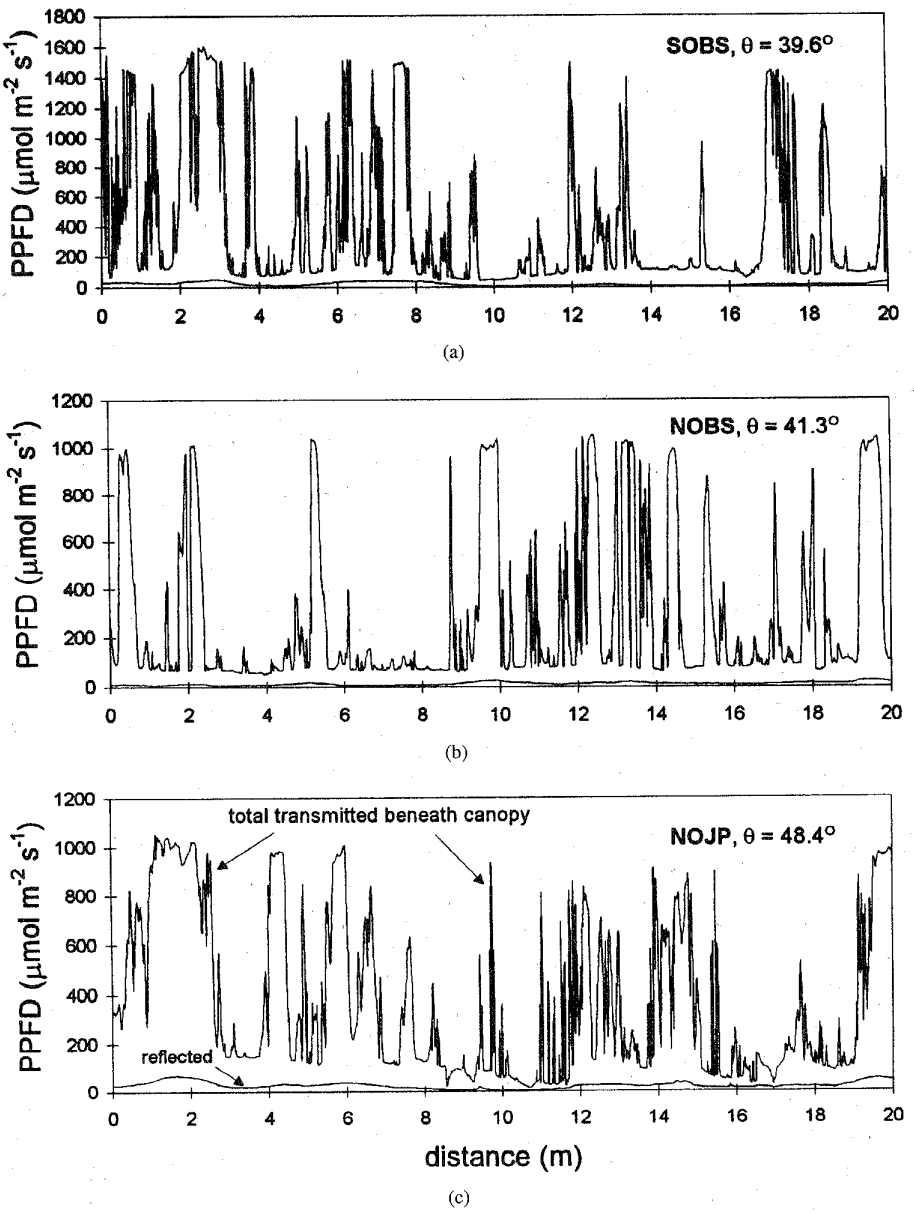


Fig. 3. Examples of TRAC measurements near the forest floor in SOBS, NOBS, and NOJP stands. Such measurements were made in six intensive sites on transects of 150–300 m long to obtain good spatial averages of the total transmitted and reflected PPFD near the forest floor.

stands where $G(\theta)$ is approximately linear against $\theta$ (Fig. 5), such curve fitting technique resulted in little error in $L_e$. However, for black spruce stands in which the relationship between $G(\theta)$ and $\theta$ is curvilinear, the error is larger but is estimated to be smaller than 5% in $L_e$ through a stepwise data elimination method. The projection coefficient $G(\theta)$ is calculated as follows:

$$G(\theta) = \frac{\cos\theta}{L_e} \ln \frac{P_{D1}}{P_{D2}}. \tag{13}$$

Comparisons between $G(\theta)$ and $G_t(\theta)$ are made in Fig. 5 for all the intensive sites. The difference between these two quantities results from the additional diffuse component included in the calculations of $G_t(\theta)$. The ratio of the above-stand to the below-stand downwelling total PPFD is smaller than the corresponding ratio for the downwelling direct PPFD due to smaller attenuation for the diffuse PPFD through the canopy, resulting in $G_t(\theta)$ being smaller than $G(\theta)$. These two quantities becomes further apart as $\theta$ increases because the diffuse PPFD decreases more slowly than the direct PPFD and becomes the dominant term at large $\theta$ values. From the pairs of $G(\theta)$ and $G_t(\theta)$ shown in Fig. 5, the mean $\beta$ value (6) for $\theta < 60°$ is shown in Table I. The individual $\beta$ values at $\theta > 60°$ are not included in the average because they have larger measurement errors and are of little importance in the calculation of daily FPAR. The $\beta$ value enables us to calculate FPAR using the more often measured quantity $L_e$ or $L_{eg}$ (5).

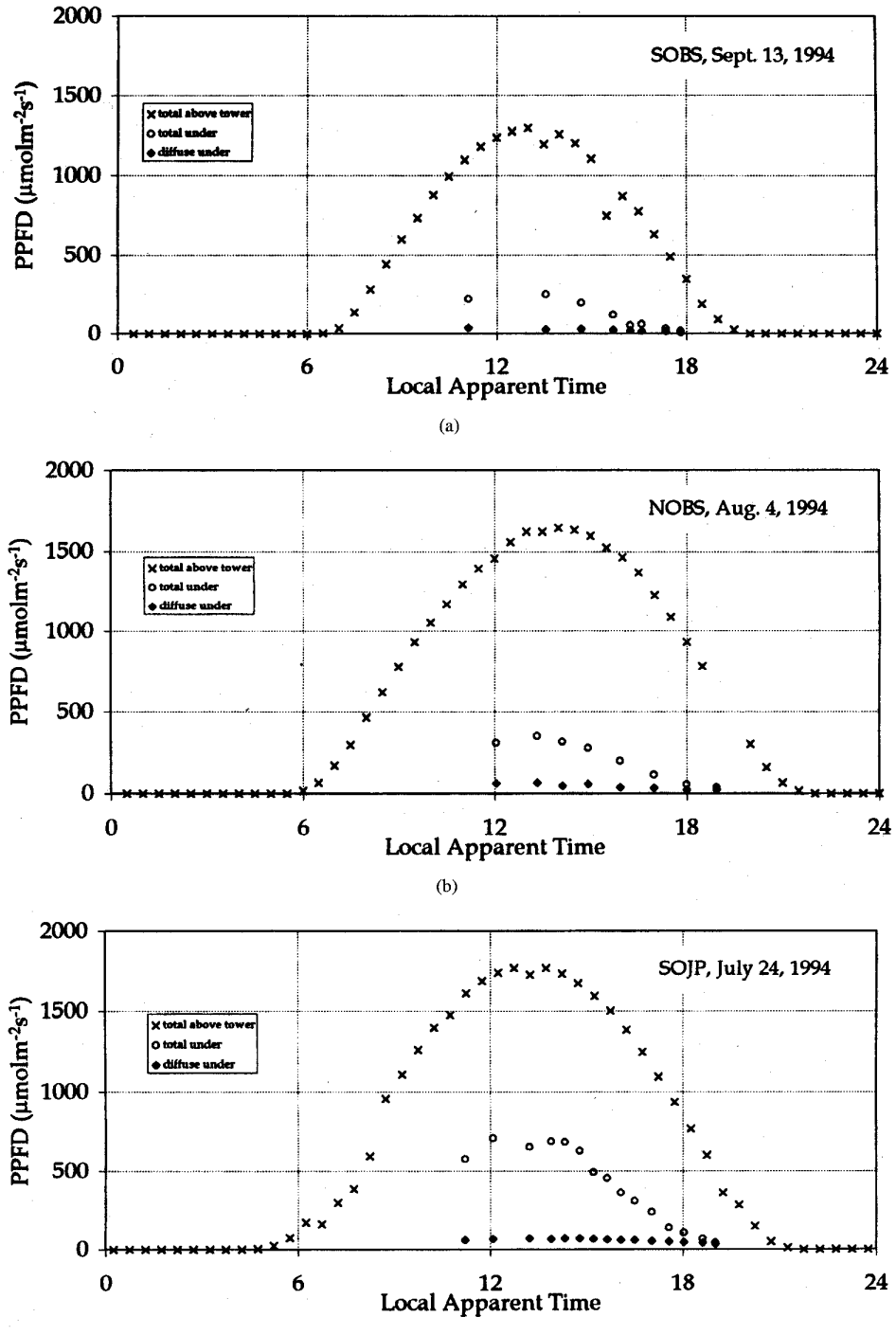


Fig. 4. Diurnal variation of the hourly mean downwelling total PPFD above the stand and the mean TRAC measurements of transmitted total and diffuse PPFD beneath the stand over the transect of length 300 m in SOBS (a) and NOBS (b) and 200 m in SOJP (c).

Table I also summarizes measurements of $L_e$ from LAI-2000 and TRAC. TRAC measurements are consistently larger than those of LAI-2000 except for SOBS. The ratio between them (last row) suggests that the LAI-2000 underestimates $L_e$ by about 20% for jack pine stands and 6% for black spruce stands compared with TRAC measurements. We believe that TRAC is an effective tool to investigate the blue light scattering effect on any $L_e$ measurements with the assumption of black leaves. This is because good spatial averages of direct and diffuse PPFD can be obtained from the TRAC transect measurements. However, uncertainties also exist in TRAC measurements because of the data extrapolation using

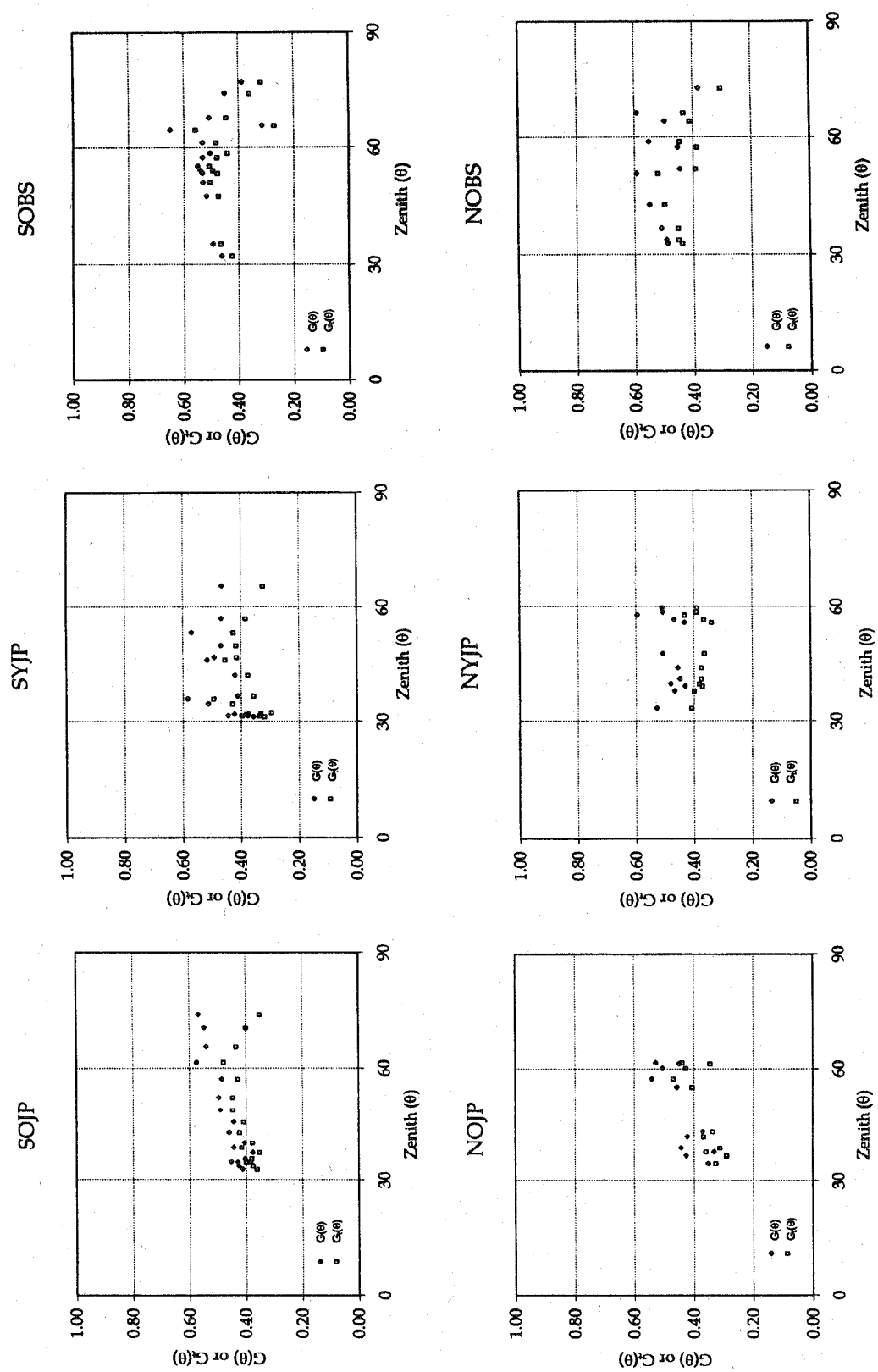


Fig. 5. The distributions of the projection coefficient for the direct PPFD ($G(\theta)$) and the projection coefficient for the total PPFD ($G_t(\theta)$) for the six intensive sites. Note the consistent difference between $G(\theta)$ and $G_t(\theta)$ and the difference in their angular distribution patterns between jack pine stands (SOJP, NOJP, SYJP, and NYJP) and black spruce stands (SOBS and NOBS).

the linear curve fitting technique. The effect is larger in jack pine stands than in black spruce stands as a result of the larger scattering coefficients as inferred from Fig. 3. These magnitudes of scattering effect may be alarming among the broad LAI-2000 users.

The deviations of both $\beta$ and the ratio from unity result from multiple scattering, and therefore they should have similar magnitudes. The ratio is determined by blue light scattering which may be slightly smaller than the scattering of total visible light affecting the $\beta$ value. The deviation of the ratio from unity is larger than that of $\beta$ because $\beta$ is confined to $\theta < 60°$ while the ratio is not. In the $L_e$ calculation using both TRAC and LAI-2000 measurements, larger weights are given to solar beam transmittance at larger zenith angles where the scattering effect is most pronounced, but for daily FPAR calculation, larger weights are given to instantaneous FPAR at smaller zenith angles. To alleviate this apparent contradiction between $L_e$ and daily FPAR calculations, it is suggested that $L_e$ measurements be confined to $\theta < 60°$ (i.e., the fifth ring of LAI-2000 be ignored). $L_e$ measured this way with the assumption of black leaves can be a surrogate for $\beta L_e$ as the first approximation for FPAR calculations. For the purpose of measuring LAI, however, measurements at large zenith angles can not be ignored and rigorous corrections for the multiple scattering effect have to be made.

The distribution patterns of $G(\theta)$ and $G_t(\theta)$ are important in the calculation of $L_e, \beta$ and FPAR. The pattern of $G(\theta)$ and hence $G_t(\theta)$ is determined by the canopy architecture. There is a distinct difference in the $G(\theta)$ pattern between jack pine (SOJP, NOJP, SYJP, and NYJP) and black spruce (SOBS, NOBS) stands. $G(\theta)$ increases almost linearly with $\theta$ in jack pine stands, but in black spruce stands the same linear trend only exists at $\theta < 50° - 60°$ and then a decreasing trend occurs at larger $\theta$ values. The jack pine pattern exhibits erectophile foliage angle distribution, i.e., more foliage is near the vertical position and less foliage is near the horizontal position compared with the spherical foliage angle distribution [36]. The black spruce pattern with a peak of $G(\theta)$ at a $\theta$ value is a typical plagiophile distribution, suggesting that the foliage is preferentially inclined to the zenith angle. We believe that the distribution patterns resulted mainly from the tree crown shape and the angle of the shoot main axis, while the needle angle may have only a small effect because black spruce and jack needles are generally closely grouped within shoots which allow little light penetration [26]. Boreal black spruce tree crowns are of conical shape at the top and cylindrical shape for the remaining part. The length of the cylindrical part is generally greater than the conical part, and the overall tree crown shape is long and narrow with foliage closely attached to main tree trunk. Boreal jack pine tree crowns have the similar shape but more irregular and have longer branches. If the tree crowns are opaque, black spruce stands would be more erectophile than the jack pine stands. However, the tree crowns contain gaps, and branch and shoot structures have important effects on the penetration of light at different zenith angles. Black spruce trees have near horizontal branches with the shoot main axis mostly oriented parallel with the plane of the branches. This architecture allows more light penetration per unit pathlength through the canopies at larger zenith angles. The $G(\theta)$ distributions found for SOBS and NOBS are similar to that found in a Douglas-fir stand with distinct horizontal branch architecture [46], although black spruce $G(\theta)$ results show less variation with $\theta$. Such horizontal branch architecture is almost absent in jack pine stands. Although the main stems of branches in the lower part of jack pine stands are near horizontal, the subbranches and the shoots are near vertical and thus reduce the planophile tendency at large $\theta$ values.

TABLE I
SUMMARY OF $\beta$ VALUES AND THE $L_e$ VALUES FROM LI-COR LAI-2000 AND TRAC FOR THE INTENSIVE SITES. THE RATIO IN THE TABLE IS THE TRAC $L_e$ DIVIDED BY THE MEAN VALUE FROM LAI-2000.

| | | | SOJP | NOJP | SYJP | NYJP | SOBS | NOBS |
|---|---|---|---|---|---|---|---|---|
| | | $\beta$ | 0.90 | 0.87 | 0.85 | 0.77 | 0.91 | 0.87 |
| LAI-2000 | IFC1 | $L_e$ | 1.54 | 1.40 | 1.31 | 1.09 | 2.04 | 2.31 |
| | IFC2 | | 1.63 | 1.43 | 1.35 | 1.09 | 2.13 | 2.39 |
| | IFC3 | | 1.53 | 1.43 | 1.37 | 1.10 | 1.97 | 2.36 |
| TRAC | IFC 1–3 | | 1.96 | 1.69 | 1.58 | 1.31 | 2.05 | 2.64 |
| | | ratio | 1.25 | 1.19 | 1.17 | 1.19 | 1.00 | 1.12 |

To support the above argument, measurements of the shoot angle distribution made in SYJP, NYJP, and SOBS are shown in Fig. 6(a)–(c). In SOBS, the majority of shoots were close to the horizontal position, i.e. the zenith angle of the shoot main axis is close to 90°. In SYJP and NYJP, the opposite occurred, i.e., shoots were more vertical than horizontal. All shoots of three trees (dominant, co-dominant, and suppressed) in SYJP and NYJP were sampled. In SOBS, a co-dominant tree was selected for the measurement and all shoots on randomly selected branches at different heights were sampled. The numbers of shoots measured in these stands are statistically significant to represent the whole stand. From visual examination, SOJP and NOJP had the similar shoot distribution pattern to those of SYJP and NYJP. The shape of black spruce and jack pine shoots can be approximated by cylinders with the length 1–3 times greater than the diameter. Hence, when the shoots are vertical, they intercept more light in near the horizontal direction than in near the vertical direction, resulting in larger projection coefficients at larger $\theta$ values. This may be the reason for the linear increase of $G(\theta)$ with $\theta$ in the jack pine stands. In black spruce stands, the increase exists at small $\theta$ values because of the dominant vertical tree crown structure, but the trend is reversed at large $\theta$ values as a result of the horizontal branch and shoot structures. These horizontal structures within the tree crown become important only when the zenith angle of the solar beam is large enough to encounter the "horizontal gaps." We believe that it is this combined vertical tree crown structure and the horizontal branch and shoot structure that produced the plagiophile distribution pattern in the black spruce stands, and this plagiophile $G(\theta)$ pattern may not be taken as the indication of a preferential inclination of foliage or needles as normally interpreted.

Fig. 7(a) shows PAR reflectivity measured above and below SOBS and SOJP stands. The above-canopy measurements were made using stationary upward and downward facing LI-COR quantum sensors mounted on the flux tower. The

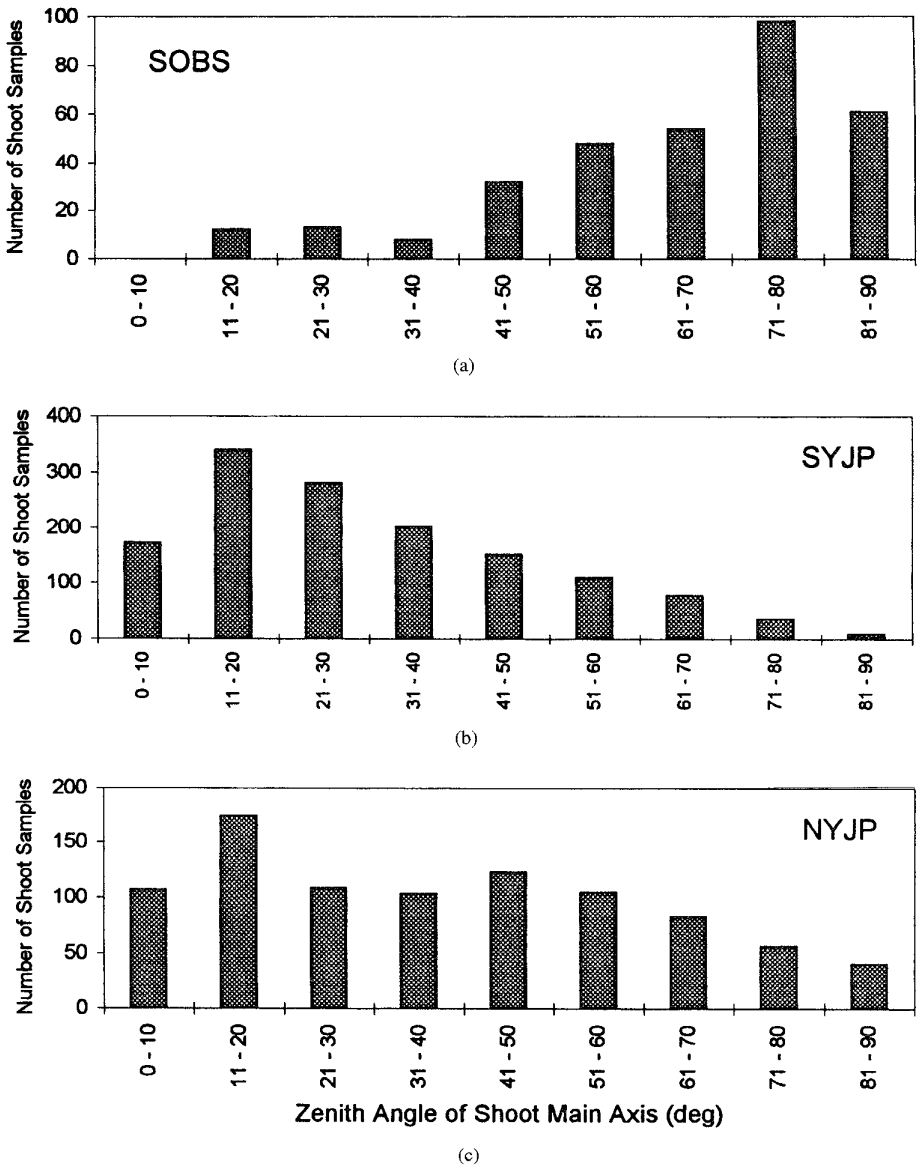


Fig. 6. The distribution of the zenith angle of conifer shoot main axis. Shoots are vertical when the zenith angle is 0° and horizontal when 90°. Note the difference between black spruce (SOBS) and jack pine (SYJP and NYJP) stands.

below-canopy PAR reflectivity is taken as the ratio of the mean reflected PAR to the mean downwelling PAR beneath the canopy measured using the TRAC along the whole transect (200 m in SOJP and 300 m in SOBS). The PAR reflectivity above both stands was almost invariant with time until $\theta > 70°$. These results suggest that while the directional reflectance depends very much on solar-target-view geometry, the hemispheric PAR albedo, averaged for all view angles, remains practically unchanged in good part of the day. Because solar irradiance on a horizontal surface becomes very small when $\theta > 70°$, this reflectivity can be treated as a constant for daily FPAR calculations. The reflectivity of SOJP was about 2% larger than that of SOBS. This is largely due to the higher forest floor reflectivity in SOJP and may also be partly caused by the higher foliage scattering coefficient as inferred from Fig. 3. The predominant forest floor cover in SOJP was lichen (*Cladina* spp) and a small percentage of blueberry (*Vaccinium myrtilloides*), bearberry (*Artostophylos uva-ursi*), and cranberry (*Vaccinium vitis-idaea*). The floor cover in SOBS consists of labrador tea (*Hylocomium splendens*) and Sphagnum moss (*Sphagnum fuscum*). Lichen appeared in the white color and was more reflective to the visible light, resulting in the larger PAR reflectivity in SOJP than in SOBS.

Fig. 7(b) exhibits all PAR reflectivity measurements in IFC-1, -2, and -3 in all the intensive sites as a function of solar zenith angle. Each point on the graph is an average of 15 000 to 30 000 data pairs taken along the transects. An important feature shown in Fig. 7(b) is that the below-canopy PAR reflectivity is invariant in the full measurable $\theta$ range. The forest floors seem to be near perfect diffuse reflectors, i.e.,

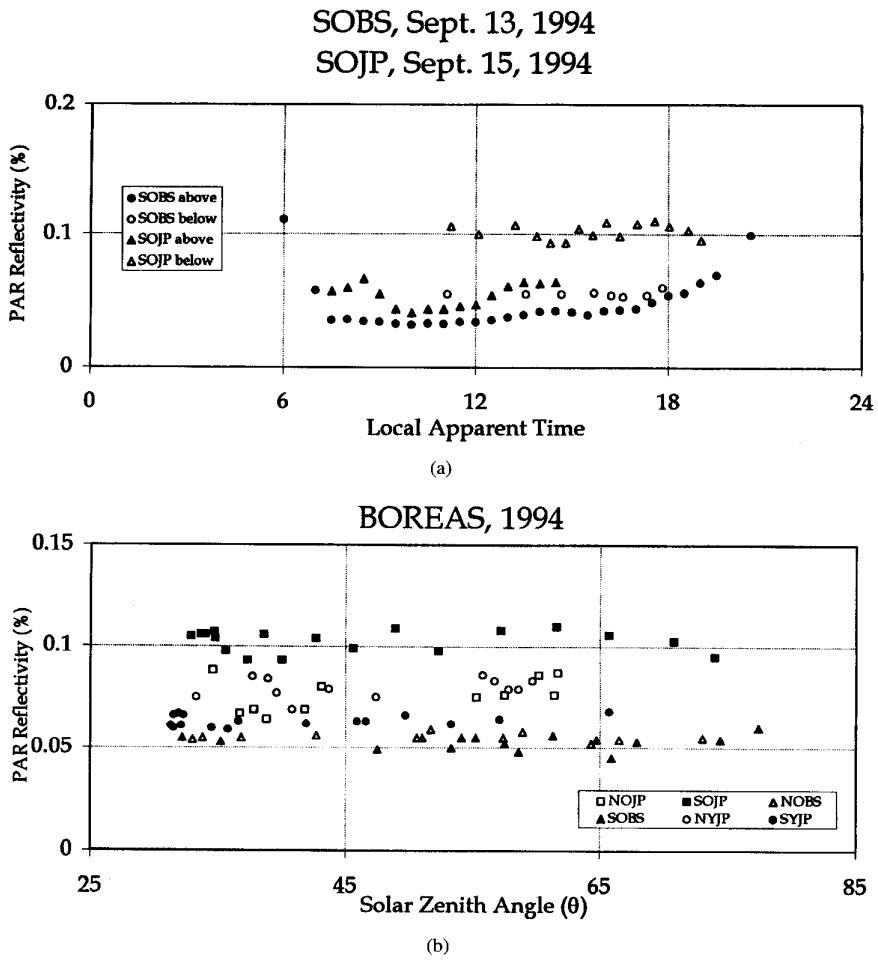


Fig. 7. (a) PAR reflectivity above and below SOJP and SOBS stands where the solar noon is at about 13:30 local apparent time. (b) PAR reflectivity of the forest floor at various solar zenith angles for the six intensive sites, calculated as the ratio of the average reflected PAR to the average transmitted PAR through the canopy over the whole transect (each point is obtained from averages of about 15 000–30 000 data points).

the Lambertian surfaces. However, it is cautioned that the measurements were done using hemispherical PAR sensors, and the invariance of the reflectivity should not be taken as the indication of uniformity of the reflected radiance in all directions. In other words, the surfaces may not be really Lambertian and the directional reflection behavior may not be ignored in other applications. SOBS and NOBS data points form the bottom line in Fig. 7(b). The forest floor in black spruce stands appeared to be most green among all stands because of the sphagnum moss and the labrador tea covers and therefore its reflectivity is close to those (2–5%) of green vegetation. The reflectivity of jack pine stands varied considerably depending on the percentage of lichens as the ground cover. The forest floor in SOJP is predominantly covered by lichens and hence has the largest reflectivity. SYJP has the lowest ground reflectivity among all jack pine stands because the ground cover is largely blueberry, cranberry, and grass with only a small fraction (estimated less than 30%) of lichens. NOJP lies in between SYJP and SOJP because it had the intermediate amounts of green vegetation cover. In conclusion, the background PAR reflectivity is small and invariant among black spruce stands and is between 6% to 11% in jack pine stands depending on the type of ground cover.

Fig. 8(a)–(c) compare measured and modeled instantaneous total FPAR on clear days for SOBS, NOBS and SOJP, respectively. Data shown in Fig. 3(a)–(c) and in Fig. 7(a)–(b) were used for the calculation of FPAR. The modeled curve was based on (5) with constant values of $\rho_1, \rho_2$ and $G_t(\theta)$. The model closely predicted the measured FPAR values, but because a constant $G_t(\theta)$ value was used for each stand, discrepancies exist between the modeled and measured results. Although $G_t(\theta)$ is similar to $G(\theta)$ and exhibits considerable variations with $\theta$ in all the intensive stands, only small errors in daily FPAR resulted from using an approximated constant for $G_t(\theta)$. In SOBS and NOBS, the largest discrepancies occurred at large $\theta$ values because of the large deviation of $G_t(\theta)$ from the assigned constant. However, these discrepancies have only a very small effect on the daily FPAR because the instantaneous FPAR at large $\theta$ values carry less weight in daily FPAR calculations (5). In SOJP, the largest discrepancies appear at around noon because of the linear increasing trend

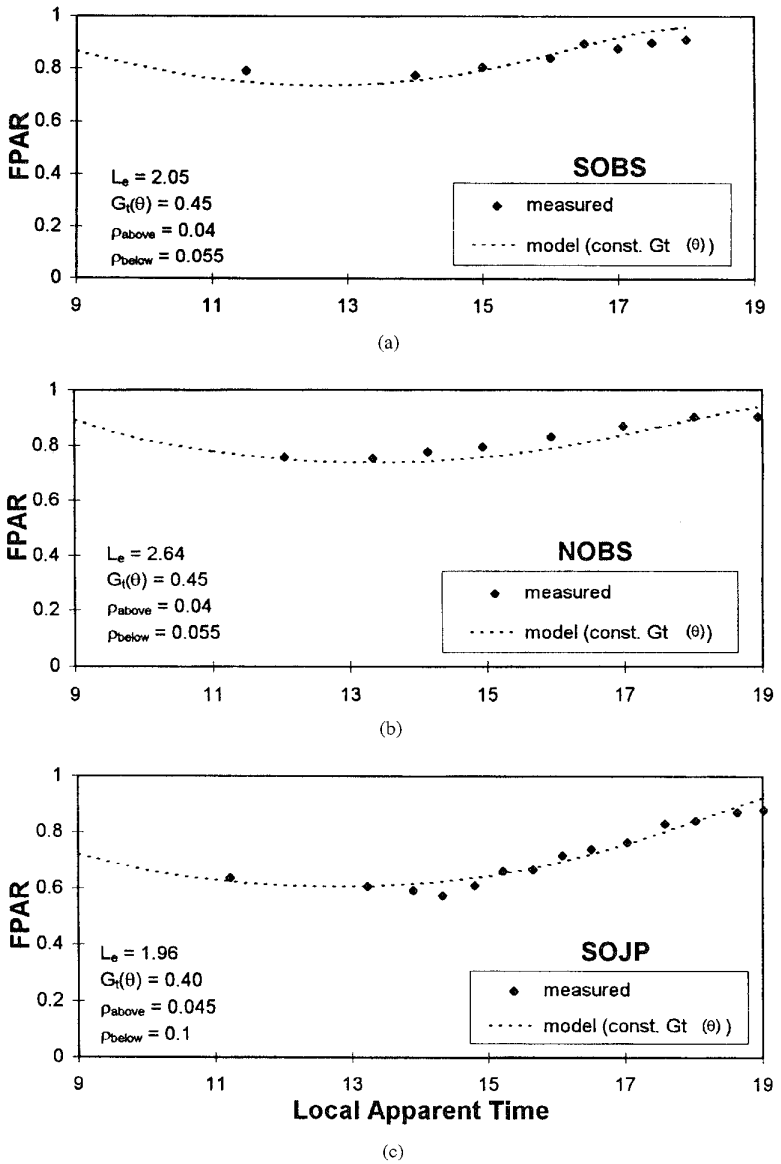


Fig. 8. Measured and modeled instantaneous total FPAR. The modeled values were obtained from (5) with constant values assigned to $G_t(\theta), \rho_1$ (above) and $\rho_2$ (below).

in $G_t(\theta)$ with $\theta$ (Fig. 5). Since the instantaneous FPAR near noon carry the largest weight in the calculation of daily FPAR, the potential problem in using a constant $G_t(\theta)$ may be larger in jack pine stands than in black spruce stands. The weighted means of the measured FPAR are 0.83, 0.81, and 0.62 for SOBS, NOBS and SOJP, respectively. They agree very well with the corresponding values of 0.82, 0.79, and 0.63 from the model.

In many cases, complete diurnal data are not available to derive $G_t(\theta)$, but $L_e$ can be easily obtained using a commercial optical instrument such as LI-COR LAI-2000. The results shown in Fig. 8(a) and (b) suggest that reasonably accurate daily FPAR for a stand can be calculated from a single $L_e$ value with constant values for $\rho_1, \rho_2$ and $G_t(\theta)$. The above-stand PAR reflectivity $\rho_1$ for conifer forest stands is generally within 1–2% of 4% and the forest floor PAR reflectivity $\rho_2$ varies very little among black spruce stands and fall within the range from 6% to 11% for jack pine stands. The accuracy in $\rho_2$ for stands with $L_e$ larger than one is of only secondary importance because the reflected PAR is further attenuated by the canopy on its way back to space. The largest potential problem in using a single $L_e$ value for daily FPAR calculations exists in $G_t(\theta)$. Chen and Cihlar [47] showed that for the same tree species, the canopy gap fraction distribution with view zenith angle can be different, depending on stand density and the tree height. This means that $G(\theta)$ and hence $G_t(\theta)$ can vary among stands of the same species, and therefore some precautions should be taken for the $G_t(\theta)$ distribution pattern. LAI-2000 not only measures $L_e$ but also stores the raw gap fraction data which can be used to obtain $G(\theta)$ for better calculation of daily FPAR in some extreme cases. As shown in Table I, it is necessary to make a 5–20% correction to LAI-

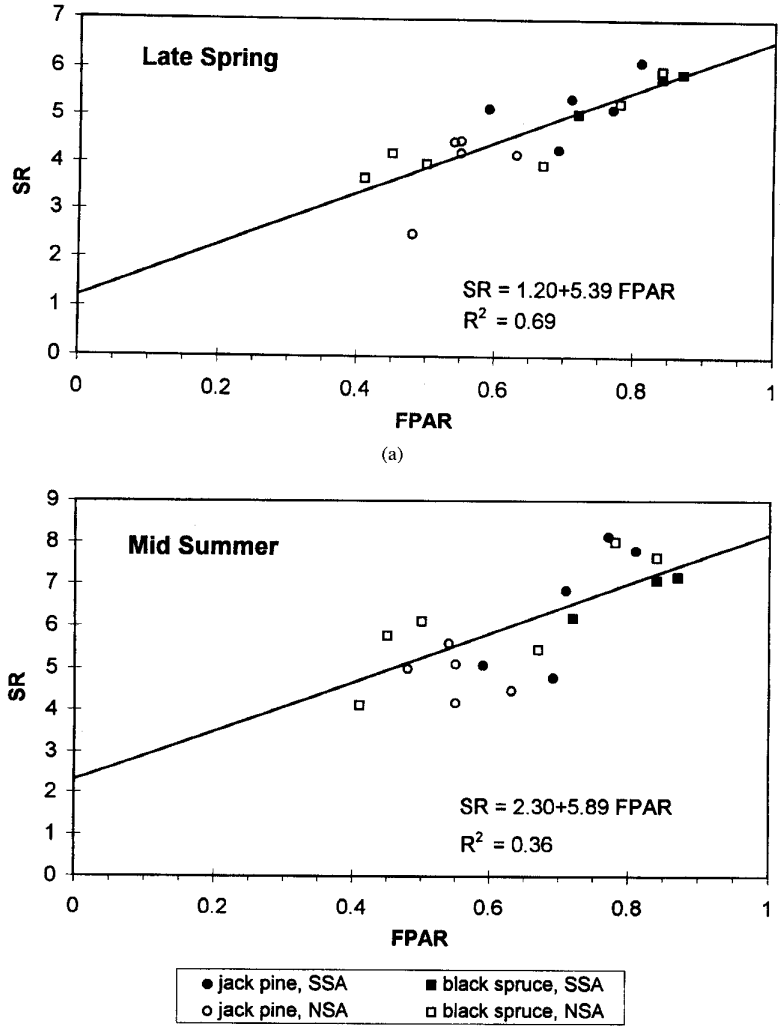


Fig. 9. Relationship between daily green FPAR and the SR obtained from Landsat TM images for (a) late spring (early June) and (b) mid-summer (mid-August).

2000 $L_e$ data for the effect of blue light multiple scattering within the canopy.

The values of $\rho_1$, $\rho_2$, and $G_t(\theta)$ obtained from the intensive sites were used for the calculation of daily green FPAR for the intensive and auxiliary sites based on $L_{eg}$ (7), where $L_{eg}$ was calculated from $L_e$ with different $\alpha$ values for different stands. The $\alpha$ values were obtained from destructive sampling, being 0.16, 028, and 0.32 for SOBS, NOJP, and SOJP, respectively [26]. They were also estimated to be 0.03 for SYJP and NYJP. The $\alpha$ value for SOBS was used for all black spruce stands, and the mean value (0.30) of NOJP and SOJP was used for all mature jack pine stands. The calculated instantaneous total FPAR from $L_e$ was compared with TRAC measurements at one or two solar zenith angles in the auxiliary sites, and they all agree within 3%.

### *B. Satellite Measurements*

Fig. 9(a) and (b) show the relationship between the daily green FPAR and the SR obtained from Landsat TM images for late spring (IFC-1) and midsummer (IFC-2), respectively. The relationships for late spring and mid-summer are considerably different. Since $L_e$ values for conifer stands varied by less than 5% from spring to summer [12], daily green FPAR calculated with the consideration for the changes in $L_e$ and solar zenith angle at noon remains practically invariant with time. However, SR changes significantly from spring to summer because of the growth of the understory and the greening of ground cover and overstory leaves (increase in the chlorophyll content). The understory growth was abundant in open stands (low $L_e$) and absent in dense stands, resulting in larger increase in SR from spring to summer in stands with lower FPAR. This seasonal change makes the sensitivity of SR to FPAR decrease from spring to summer. This decrease in sensitivity is largely responsible for the decrease in the significance of regression ($R^2$). The variation in the understory signal contribution in different stands may be the major cause of the large scatter of the data points. The summer images used in Fig. 9(b) were acquired eight and nine years prior to the field data collection. The time difference may have also contributed to the scatter, but the contribution is believed to

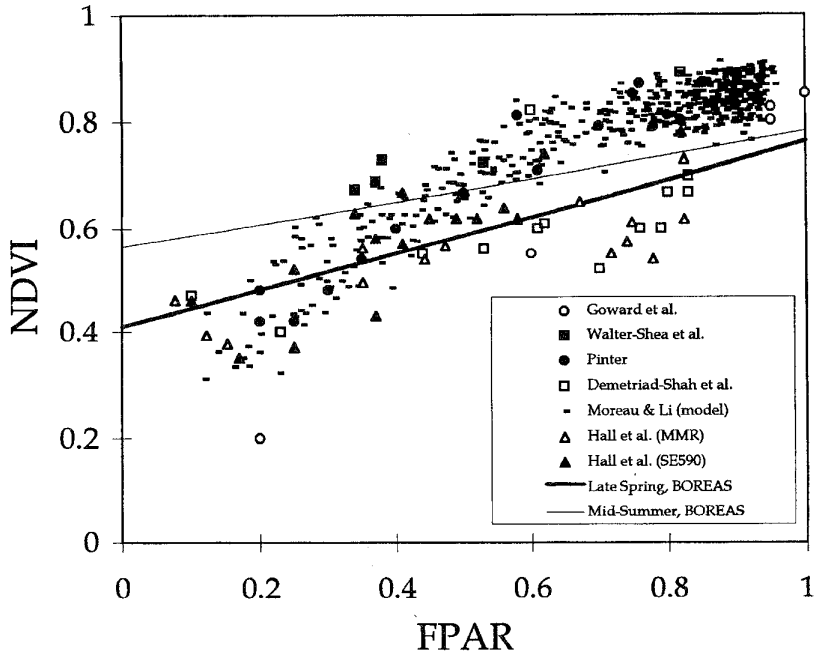


Fig. 10. Comparison of present results (thin and thick lines) for boreal forests with modeled values of Moreau and Li [21] and previous results for a tallgrass prairie [48], [49], [23], an alfalfa field [24], and temperate forests and grassland [25].

be small because of the stable conditions of the mostly mature stands (the youngest stands SYJP and NYJP were both 28 years old). The corresponding linear regression results using NDVI are as follows:

$$\text{late spring:} \quad NDVI = 0.41 + 0.35\, F_{gd} \qquad (R^2 = 0.56)$$

$$\text{midsummer:} \quad NDVI = 0.57 + 0.22\, F_{gd} \qquad (R^2 = 0.30).$$

The sensitivity of NDVI to $F_{gd}$, i.e., coefficient of $F_{gd}$, is also considerably less in summer than in spring. These results suggest that spring images are more useful for determining the FPAR values for the overstory. From field spectral measurements [50], NDVI for the background (understory and moss ground cover) in these stands was calculated to be in the ranges of 0.35–0.5 and 0.40–0.60 for late spring and midsummer, respectively [47]. The intercepts of the linear regressions, being 0.41 and 0.57 for the late spring and midsummer, respectively, fall within the corresponding ranges. Landsat observes the earth's surface within a few degrees of the nadir. If these relationships are applied to NDVI obtained under different sun–target–view geometry, corrections to NDVI for the view and solar angles are necessary.

These NDVI–$F_{gd}$ relationships are plotted in Fig. 2 of Moreau and Li [21] for the comparison with previous results (Fig. 10). Moreau and Li's results were obtained using a multilayer radiative transfer model assuming random leaf angular and spatial distributions. The model simulates FPAR-NDVI relationship using a range of ground and leaf reflectivities in the visible and near infrared bands. The modeled results are similar to those of Myneni and Williams [20] for homogeneous canopies. The plotted data points include those of Hall *et al.* [23], Walter–Shea *et al.* [48], and Demetriades–Shah *et al.* [49] from the same tallgrass prairie in Kansas, Pinter [24] from an alfalfa field, and Goward *et al.* [25] from temperate forests and grassland. There are considerable discrepancies between the various results for the prairie: Walter–Shea *et al.*'s results have the largest NDVI for the same FPAR, and Demetriades–Shah *et al.* are among those with the smallest NDVI. The discrepancies may be a result of the optical sensor differences. Both sets of Hall *et al.*'s results, one from the Barnes Modular Multiband Radiometer (MMR) and the other from the Spectron Engineering Model 590 (SE590), were measured at the same sites from a helicopter, but they are considerably different. The difference was mainly attributed to different bandwidth choices of the sensors [23]. The alfalfa FPAR data compare well with the results of Walter–Shea *et al.* [48], Moreau and Li's model, and another data set (not plotted) by Wiegand *et al.* [22] for wheat, indicating that the assumptions for the random leaf angular and spatial distributions may be appropriate for some agricultural crops and grassland. However, the relationships of NDVI and FPAR predicted using models of this type (including those of Myneni and Williams [20]) do not compare well with those (thin and thick lines in Fig. 10) from the present study. The major differences are: 1) the measured NDVI values in boreal forests with small FPAR are larger than the modeled values due to strong signals from the background (understory and moss cover) in the open stands [47] [50], suggesting the background NDVI value needs to be adjusted to account for the difference; and 2) at large FPAR values, the measured NDVI is smaller than the modeled NDVI. In Moreau and Li's model, the input reflectivity and transmissivity were both in the range from 0.05 to 0.10 for the visible band and were 0.35–0.55 and 0.45–0.55, respectively, for the near infrared band. These ranges cover fairly well the optical properties of conifer needles (although

conifer needles have lower transmissivity than the input), but the modeled NDVI is consistently larger than the measured NDVI at large FPAR values. The difference may be beyond the tuning of the model by adjusting the input parameters. The intrinsic problem may lie in the model assumption for the leaf spatial distribution. In open boreal forests, tree crowns cast shadows on the ground and have shadows on the shaded side that can be seen by optical sensors above. Shadows typically have lower NDVI than sunlit leaves and background [51]. Compared with canopies with no such tree crown structure, more shadows can be seen in conifer stands for the same amount of sunlit leaves (i.e., more sunlit leaves can lie behind other leaves in the viewing direction), resulting in smaller NDVI for the whole stand. This comparison suggests that canopy architecture can not be ignored in modeling the relationship between satellite spectral measurements and biophysical parameters of boreal forests.

## VI. Summary

A simple formula for calculating daily green FPAR for forest stands is proposed and validated using field data from six intensive sites and 14 auxiliary sites in black spruce and jack pine stands. The formula is based on a single stand parameter: the effective green LAI, which is easily obtained using optical instruments after a small adjustment to remove the contribution of standing woody material. The formula uses constant values for the above and below stand PAR reflectivities, and the projection coefficient for total (direct and diffuse) PAR based on the following experimental evidence: 1) PAR reflectivity measured above forest stands showed very small variation until the solar zenith angle $\theta$ was larger than 70°, 2) PAR reflectivity of the forest floor varied very little with $\theta$, and 3) the combined effect of tree crown, branch, and shoot architecture makes both jack pine and black spruce canopies considerably depart from the spherical foliage angle distribution only when $\theta > 60°$. In the calculation of daily FPAR, the effect of this departure is reduced because small weights are given to the instantaneous FPAR at large $\theta$ values.

The correlation between daily green FPAR and SR or NDVI obtained from Landsat 5 TM images was found to be better in late spring than in midsummer. The spring images were better for determining the overstory FPAR because the effect of the understory and moss cover was less in this season. The relationships between FPAR and NDVI obtained from this study were considerably different from those from a tallgrass prairie and other ecosystems. The differences may be taken as an indication of the importance of the background (understory and ground cover) and the canopy architecture (tree shadows and sunlit crowns) in the determination of FPAR from remote sensing data.

## Acknowledgment

The author is indebted to Dr. J. Cihlar for useful discussions and participation in part of the field experiment. Dr. Z. Li participated in part of IFC-3 and carefully reviewed the manuscript before submission to this journal. M. Guilbeault assisted in image and field data analysis and archiving and part of the field experiment. S. Leblanc provided comments on the manuscript. The above mentioned scientists are at the Canada Centre for Remote Sensing. Dr. P. Jarvis of Edinburgh University, Dr. D. Baldocchi of Oakridge Research Laboratory, and Dr. S. Wofsy of Harvard University kindly provided above-stand downwelling and upwelling data for SOBS, SOJP, and NOBS, respectively.

## References

[1] P. P. Tans, I. Y. Fung and T. Takahashi, "Observational constraints on the global atmospheric $CO_2$ budget," *Sci.* vol. 247, pp. 1431–1438, 1990.

[2] S. W. Running and J. C. Coughlan, "A general model of forest ecosystem processes for regional applications. I. Hydrologic balance, canopy gas exchange and primary production processes," *Ecol. Model.*, vol. 42, pp. 125–154, 1988.

[3] G. B. Bonan, "Importance of leaf area index and forest type when estimating photosynthesis in boreal forests," *Remote Sens. of Environ.*, vol. 43, pp. 303–314, 1993.

[4] P. J. Sellers, Y. Mintz, Y. C. Sud, and A. Dalcher, "A simple biosphere model (SiB) for use within general circulation models," *J. Atmos. Sci.*, vol. 43, pp. 505–531, 1986.

[5] R. E. Dickinson, A. Henderson–Sellers, and P. J. Kennedy, "Biosphere-atmosphere transfer Scheme (BATS) Version le as coupled to the NCAR Community Climate Model," NCAR Technical Note, NCAR /TN-387, Natl. Center for Atmos. Res. Boulder, CO, 1993.

[6] P. J. Sellers *et al.*, "BOREAS-Boreal Ecosystems-Atmosphere Study: global change biosphere-atmosphere interactions in the boreal forests biome-science plan," no. 923, NASA/GSFC, Greenbelt, MD, pp. 67, 1991.

[7] D. W. Deering, "Rangeland reflectance characteristics measured by aircraft and spacecraft sensors," Ph.D. dissertation, Texas A&M University, College Station, TX, 1978, pp. 338.

[8] C. F. Jordan, "Derivation of leaf area index from quality of light on the forest floor," *Ecology*, vol. 50, pp. 663–666, 1969.

[9] P. J. Sellers *et al.*, "A global 1°*1° NDVI data set for climate studies. Part 2: The generation of global fields of terrestrial biophysical parameters from the NDVI," *Int. J. Remote Sens.* vol. 15, pp. 3519–3545, 1994.

[10] F. G. Hall, J. R. Townshend and E. T. Engman, "Status of remote sensing algorithms for estimation of land surface state parameters," *Remote Sens. Environ.*, vol. 51, pp. 138–156, 1995.

[11] S. W. Running, E. R. Hunt, R. Nemani, and J. Glassy, "MODIS LAI and FPAR," 19 pp. MODIS algorithm doc., NASA, 1994.

[12] J. M. Chen, "Evaluation of vegetation indices and a simple ratio for boreal applications," *Can. J. Remote Sensing,* vol. 22, pp. 229–242, 1996.

[13] A. R. Huete, "A soil adjusted vegetation index (SAVI)," *Remote Sens. Environ.*, vol. 25, pp. 295–309, 1988.

[14] J. Qi *et al.*, "A modified soil adjusted vegetation index," *Remote Sens. Environ.*, vol. 48, pp. 119–126, 1994.

[15] J. G. P. W. Clevers, "The applications of a weighted infrared-red vegetation index for estimating leaf area index by correcting for soil moisture," *Remote Sens. Environ.*, vol. 29, pp. 25–37, 1989.

[16] B. Pinty and M. M. Verstrate, "GEMI: a nonlinear index to monitor global vegetation from satellites," *Vegetatio*, vol. 10, pp. 15–20, 1992.

[17] N. S. Goel and W. Qin, "Influences of canopy architecture on relationships between various vegetation indexes and LAI and FPAR: a computer Simulation," *Remote Sens. Rev.*, vol. 10, pp. 309–347, 1994.

[18] J.-L. Roujean and F. M. Breon, "Estimating PAR absorbed by vegetation from bidirectional reflectance measurements," *Remote Sens. of Environ.*, vol. 51, pp. 375–384, 1995.

[19] S. N. Goward and K. E. Huemmrich, "Vegetation canopy PAR absorptance and the Normalized Difference Vegetation Index: an assessment using the SAIL model," *Remote Sens. Environ.*, vol. 39, pp. 119–140, 1992.

[20] R. B. Myneni and D. L. Williams, "On the relationship between FAPAR and NDVI," *Remote Sensing of Environ.*, vol. 49, pp. 200–211, 1994.

[21] L. Moreau and Z. Li, "A new approach for remote sensing of canopy absorbed photosynthetically active radiation. Part 2: A radiative transfer simulation study in canopies," *Remote Sens. Environ.*, vol. 55, 1996.

[22] C. L. Wiegand, A. J. Richardson, D. E. Escobar, and A. H. Gerbermann, "Vegetation indexes in crop assessments," *Remote Sens. Environ.* 35:105–119, 1991.

[23] F. G. Hall *et al.*, "Satellite remote sensing of surface energy balance: successes, failures and unresolved issues in FIFE," *J. Geo. Phys. Res.*, vol. 97, pp. D17:19,061–19,090, 1992.
[24] P. Pinter, "Solar angle independence in the relationship between absorbed PAR and remotely sensed data for alfalfa," *Remote Sens. Environ.*, vol. 46, pp. 19–25, 1993.
[25] S. K. Goward, K. Huemmrich, and R. Waring, "Visible-near infrared spectral reflectance of landscape component in western Oregon," *Ecolog. Applicat.*, vol. 4, pp. 322–343, 1994.
[26] J. M. Chen, "Optically-based methods for measuring seasonal variation of leaf area index in boreal conifer stands," *Agric. For. Meteorol.* vol. 50, pp. 135–163, 1996.
[27] N. S. Goel, I. Rozenhnal, and R. L. Thompson, "A computer graphics based model for scattering from objects of arbitrary shapes in the optical region," *Remote Sens. Environ.*, vol. 36, pp. 73–104, 1991.
[28] R. B. Myneni, "Modeling radiative transfer and photosynthesis in three-dimensional vegetation canopies," *Agric. For. Meteorol.* vol. 55, pp. 323–344, 1991.
[29] X. Li, A. Strahlar, and C. E. Woodcock, "A hybrid geometric optical-radiative transfer approach for modeling albedo and directional reflectance of discontinuous canopies," *IEEE Trans. Geosci. Remote Sens.*, vol. 33, pp. 466–480, 1995.
[30] J. M. Chen and J. Cihlar, "Plant canopy gap size analysis theory for improving optical measurements of leaf area index of plant canopies," *Appl. Opt.*, vol. 34, pp. 6211–6222, 1995.
[31] ——, "Quantifying the effect of canopy architecture on optical measurements of leaf area index using two gap size analysis methods," *IEEE Trans. Geosci. Remote Sens.*, vol. 33, pp. 777–787, 1995.
[32] T. Nilson, "A theoretical analysis of the frequency of gaps in plant stands,"*Agric. Meteorol.*, vol. 8, pp. 25–38, 1971.
[33] J. M. Chen and T. A. Black, "Defining leaf area index for nonflat leaves," *Plant, Cell and Environ.*, vol. 15, pp. 421–429, 1992.
[34] J. M. Norman and G. S. Campbell, "Canopy structure," in *Plant Physiological Ecology. Field Methods and Instrumentation,* R. W. Pearcy, J. Ehleringer, H. A. Mooney, and P. W. Rundel, Eds. New York: Chapman and Hall, 1989, pp. 300–325.
[35] J. M. Chen and T. A. Black, "Measuring leaf area index of plant canopies with branch architecture," *Agric. For. Meteorol.*, vol. 57, pp. 1–12, 1991.
[36] J. Ross, *The Radiation Regime and Architecture of Plant Stands.* London: Junk, 1981, 391 pp.
[37] T. A. Black, J. M. Chen, X. Lee, and R. M. Sagar, "Characteristics of shortwave and longwave irradiances under a Douglas-fir forest stand," *Can. J. For. Res.*, vol. 21, pp. 1020–1028, 1991.
[38] J. M. Norman, "Modeling the complete crop canopy," in *Modification of the Aerial Environment of Plants,* B. J. Bartifield and J. F. Gerber, Eds. St. Joseph, MI: Amer. Soc. Agricult. Engineers, 1979, pp. 249–277.
[39] D. M. Gates, *Biophysical Ecology.* New York: Springer-Verlag, 1980, 611 p.
[40] M. J. Apps *et al.*, "BOREAS biometry and auxiliary sites," Rep. North. Forestry Centre, Edmonton, Alta., Canada, 1994.
[41] J. M. Murphy, "Standard Landsat 4,5 and 6 TM CCT format specification," Tech. Rep. DMD-TM 82-249E, Canada Ctr. for Remote Sens., Geomatics Canada, 1991.
[42] D. Tanré *et al.*, "Simulation of the Satellite Signal in the Solar Spectrum," Laboratoire d optique atmosphérique, Université des sciences et techniques de lille, 59655 Villeneuve d Ascq Cédex, France, 1986, 343 pp.
[43] P. M. Teillet and R. P. Santer, "Terrain elevation and sensor altitude dependence in a semi-analytical atmospheric code," *Can. J. Remote Sens.*, vol. 17, pp. 36–44, 1991.
[44] J. B. Miller, "A formula for average foliage density," *Aust. J. Bot.*, vol. 15, pp. 141–144, 1967.
[45] A. R. G. Lang, "Simplified estimate of Leaf area index from transmittance of sun's beam," *Agric. For. Meteorol.*, vol. 41, pp. 179–186, 1987.
[46] J. M. Chen and T. A. Black, "Measuring leaf area index of plant canopies with branch architecture," *Agric. For. Meteorol.*, vol. 57, pp. 1–12, 1991.
[47] J. M. Chen and J. Cihlar, "Retrieving leaf area index of boreal conifer forests using Landsat TM images," *Remote Sens. Environ.*, vol. 55, pp. 153–162, 1996.
[48] E. Walter–Shea *et al.*, "Biophysical properties affecting vegetative reflectance and absorbed photosynthetically active radiation at FIFE site," *J. Geophys. Res.*, vol. 97D, pp. 18925–18934, 1992.
[49] T. H. Demetriades–Shah, E. T. Kanemasu, and I. D. Flitcroft, "Comparison of ground- and satellite-based measurements of the fraction of photosynthetically active radiation intercepted by tallgrass prairie," *J. Geophys. Res.*, vol. 97D, pp. 18947–18950, 1992.
[50] H. P. White *et al.*, "Seasonal change in mean understory reflectance for boreal sites: preliminary results," in *Dig. 17th Canadian Symp. on Remote Sens.,* Saskatoon, Canada, 1995.
[51] F. G. Hall, Y. E. Shimabukuro, and K. F. Huemmrich, "Remote senisng of forest biophysical structure in boreal stands of Picea Mariana using mixture decomposition and geometric reflectance models," *Ecolog. Modeling*, 1996.

**Jing M. Chen** received the B.Sc. degree from the Nanjing Institute of Meteorology, P.R. China, and the Ph.D. degree from the University of Reading, U.K., in 1982 and 1986, respectively.

He is currently a Research Scientist at the Canada Centre for Remote Sensing (CCRS) and an Adjunct Professor at the University of Ottawa, Canada. His main research interests have been in turbulent and radiative transfer processes associated with plant canopies. He is currently engaged in research on applications of optical and microwave remote sensing techniques to boreal ecosystems. He has been a principal investigator in Boreal Ecosystems-Atmosphere Study and other projects.